Cite this: *Dalton Trans.*, 2018, **47**, 16350

The development of a new approach toward lanthanide-based OLED fabrication: new host materials for Tb-based emitters†

Andrey N. Aslandukov,^a Valentina V. Utochnikova,^{a,b} Dmitry O. Goriachiy,^c Andrey A. Vashchenko,^c Dmitry M. Tsymbarenko,^a Michael Hoffmann,^d Marek Pietraszkiewicz^e and Natalia P. Kuzmina^a

To develop the recently proposed approach toward host selection for lanthanide-based emitters, four phosphine oxides PO = PO1–PO4 were investigated which are able to both increase the electron mobility and to sensitize terbium luminescence. New highly soluble and brightly luminescent terbium complexes TbCl₃(PO)·H₂O and Tb(pobz)₃(PO)·(CH₃)₂CO (pobz[−] = phenoxybenzoate) with a quantum yield of up to 100% were synthesized and thoroughly characterized. To study the electroluminescence properties of these materials, a series of solution-processed OLED devices were fabricated and their heterostructures were selected based on the HOMO and LUMO energies of PO1–PO4, which were carefully assessed by the combination of DFT and TDDFT methods. Thus, the effectiveness of the proposed approach was proved, and the influence of the anionic ligand was shown. The maximum OLED luminance reached 75 Cd m^{−2}, which is a high value for solution-processed OLEDs based on terbium complexes.

Received 17th July 2018,
Accepted 19th October 2018

DOI: 10.1039/c8dt02911c

rsc.li/dalton

Introduction

Organic light-emitting diodes (OLEDs) have drawn intense attention during the past few decades due to their potential applications in solid-state lighting and flat-panel displays. The standard method for fabricating organic light-emitting diodes (OLEDs) based on small molecules is vapor deposition of materials through a series of physical shadow masks.^{1,2} However, this process has critical drawbacks including considerable loss of the expensive materials during evaporation and high manufacturing costs. The best way to improve the efficiency of the process and reduce the production costs is to use solution processing of OLED materials.²

At the same time, the efficiencies of solution-processed OLEDs are generally lower than those of vacuum-deposited OLEDs.^{3,4} This is primarily related to the fast degradation of the device. Lee *et al.* showed that the crucial factor determin-

ing the device lifetime is the film morphology and the packing density. Since the molecules in the films obtained by solution processing are not as closely packed as those in the vacuum-based layers, solvent impurities may remain inside the solution-processed films and oxygen can diffuse into the film more easily.⁴

However, due to the further optimization of the film deposition process, *e.g.* selection of an optimal solvent, spin-coating speed and temperature, for certain materials, it is already possible to obtain OLEDs that are only slightly inferior to vacuum-deposited analogues.⁵ Thus, a further search for new materials for solution-processed OLEDs is an important task.

As materials, we propose coordination compounds of lanthanides. Because of the special mechanism of luminescence,⁶ the triplet excitons are involved in the luminescence processes, and lanthanide narrow emission bands (down to FWHM = 10 nm) guarantee a high purity of light. At present, the best results in OLEDs based on lanthanide complexes were obtained using mixed-ligand beta-diketonate complexes deposited from the gas phase.^{7,8} However, beta-diketonates are unstable under current. Therefore, a promising class of anionic ligands are aromatic carboxylates, since they are stable⁹ and exhibit quantum yields of up to 100%.¹⁰ However, they usually do not possess the intrinsic mobility of charge carriers. To solve this problem, an additional host material that must demonstrate high mobility, for example electronic, and

^aM.V. Lomonosov Moscow State University, 1/3 Leninskye Gory, Moscow 119991, Russia. E-mail: valentina.utochnikova@gmail.com

^bEVOLVED Ltd, 1A-24 Puškina iela, Riga LV-1050, Latvia

^cP.N. Lebedev Physical Institute, Leninsky prosp. 53, Moscow 119992, Russia

^dFraunhofer Institute for Organic Electronics, Electron Beam and Plasma Technology FEP, Maria-Reiche-Straße 2, 01109 Dresden, Germany

^eInstitute of Physical Chemistry, Polish Academy of Sciences, Kasprzaka 44/52, 01-224 Warsaw, Poland

† Electronic supplementary information (ESI) available. See DOI: 10.1039/c8dt02911c

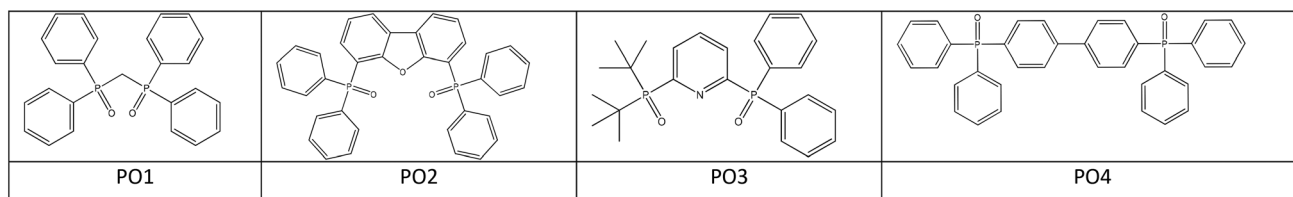


Fig. 1 Investigated host materials.

effectively transfer energy to the emitter is widely utilized. The classical approach to the choice of the host material is based on the host \rightarrow ligand energy transfer, but in the case of lanthanide compounds, this transfer implies a large Stokes shift, which leads to a loss of the OLED efficiency. Thus, we have recently proposed a new approach to the selection of such a host that will transfer energy directly to the luminescent ion due to coordination.¹¹

In the present work, we investigate four new host materials, able to serve as ligands (Fig. 1). Due to the presence of a electron-depleted system, we expect them to possess electronic mobility; indeed, PO2 and PO4 were already tested as host materials in iridium-based OLEDs.^{12,13} While the presence of the P=O fragment makes them capable of forming complexes with the lanthanide ion,^{14,15} particularly PO1 and PO4 were used to form complexes with Tb³⁺.^{16,17} As the emitting ion, Tb³⁺ was selected because phosphine oxides are known to sensitize the terbium luminescence efficiently.

Since the electroexciton will be generated on a host material that is directly capable of transferring energy to the lanthanide ion, the role of the anionic ligand becomes unobvious. To determine the role of the anionic ligand, we have chosen two different anions: the chloride anion, which is not capable of sensitizing the terbium luminescence, and the *o*-phenoxybenzoate anion (pobz⁻), which is known for its very effective sensitization of the terbium luminescence (QY(Tb(pobz)₃(H₂O)₂) = 96%) and at the same time it does not possess the intrinsic charge carrier mobility.¹⁸

Results and discussion

Synthesis and complex composition

TbCl₃(PO)·H₂O complexes were obtained by a reaction between an excess of TbCl₃·6H₂O and the corresponding PO in ethanol, followed by evaporation of the reaction mixture to dryness and washing with water to avoid the impurity of TbCl₃·6H₂O. This resulted in the formation of monohydrated complexes, which were analyzed using the thermal analysis data. While Tb(pobz)₃(PO)·(CH₃)₂CO (PO = PO1–PO4) complexes were obtained as a precipitate from a water–acetone mixture, which leads to a different solvate composition.

To determine this solvate composition, the thermal analysis data with the simultaneously recorded MS profiles were used (Fig. 2). The profiles of carbon dioxide (*m/z* = 44) and water (*m/z* = 18) evolution were very similar in shape and reflected

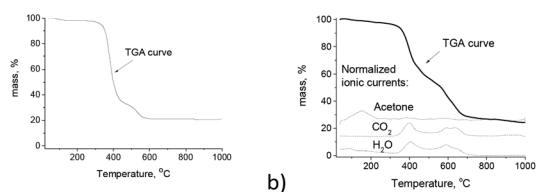
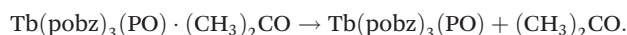


Fig. 2 (a) TGA curve of TbCl₃(PO1)·H₂O and (b) TGA curve and simultaneously detected evolution of the gaseous decomposition products of Tb(pobz)₃(PO4)·(CH₃)₂CO. Normalized MS profiles are given for *m/z* 18 (H₂O), 44 (CO₂), and 58 (acetone).

the contribution of complex thermal decomposition in the temperature range of 325–740 °C. No additional temperature points corresponding to the local concentration maxima at lower temperature were detected in the H₂O evolution profile (Fig. 2b), indicating no coordinated water molecules. Unlike water, the acetone evolution profile (*m/z* = 58) demonstrated a pronounced concentration maximum at 155 °C, corresponding to its removal according to the reaction:



Such a high temperature point might be the consequence of the chemical bond between the acetone molecule and Tb(pobz)₃(PO). Thus, the nature of the solvent was determined from the MS profiles, while the corresponding weight loss allowed determining the number of the coordinated acetone molecules.

The TGA data also indicated the absence of the PO impurity, which is indirectly supported by the PXRD data, at least for PO2 and PO4. Indeed, all the Tb(pobz)₃(PO)·(CH₃)₂CO complexes are amorphous (Fig. S22†), while PO complexes (PO = PO1–PO4) are crystalline (Fig. S19–21†), which proves the absence of the free neutral ligand PO impurity.

In the case of both TbCl₃(PO)·H₂O and Tb(pobz)₃(PO)·(CH₃)₂CO, only one neutral ligand molecule (PO) is coordinated, which is confirmed from the TGA data. In the case of Tb(pobz)₃(PO)·(CH₃)₂CO, this conclusion is also supported by the ¹H NMR spectroscopy data, based on the ratio of the integrated intensities of the non-overlapping signals of neutral ligands PO1–PO4 and the anionic ligand pobz⁻. Since the Tb³⁺ ion has strong paramagnetic ion effects¹⁹ and the NMR spectra of its complexes are usually not quantitative due to strong signal broadening,²⁰ ¹H NMR analysis was carried out for La(pobz)₃(PO)·(CH₃)₂CO complexes, synthesized by the

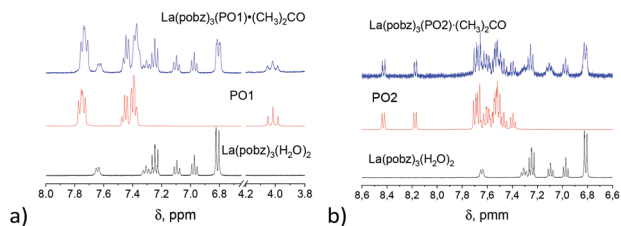


Fig. 3 ^1H NMR spectra of $\text{La}(\text{pobz})_3(\text{PO})\cdot(\text{CH}_3)_2\text{CO}$, PO and $\text{La}(\text{pobz})_3(\text{H}_2\text{O})_2$, PO = (a) PO1 and (b) PO2 in $\text{DMSO}-d_6$.

same reaction (Fig. 3). The ionic radius of La^{3+} is larger than that of Tb^{3+} , which suggests that if the La^{3+} coordination sphere is saturated due to the coordination of only one neutral PO ligand in the $\text{La}(\text{pobz})_3(\text{PO})\cdot(\text{CH}_3)_2\text{CO}$ complexes, then the coordination sphere of the terbium ion will also be saturated with only one molecule of PO.

The ^1H NMR spectra of the $\text{La}(\text{pobz})_3(\text{PO})\cdot(\text{CH}_3)_2\text{CO}$ complexes represent the superposition of the ^1H NMR spectra of $\text{La}(\text{pobz})_3(\text{H}_2\text{O})_2$ and of the corresponding PO. The ratio of the integrated intensities of the signals indicate the 3 : 1 ratio of the pobz $^-$ and PO ligands, which confirms the assigned composition. It is also worth noting that due to the coordination to the La^{3+} ion, the PO signals in the spectrum of the complex are slightly shifted in comparison with the spectrum of the free ligand (*i.e.* from 7.75 ppm for PO1 to 7.73 ppm for $\text{La}(\text{pobz})_3(\text{PO1})\cdot(\text{CH}_3)_2\text{CO}$), indicating the coordination of the neutral ligand by La^{3+} in DMSO , while the signals of pobz $^-$ protons are almost not shifted from $\text{La}(\text{pobz})_3(\text{H}_2\text{O})_2$ to $\text{La}(\text{pobz})_3(\text{PO})\cdot(\text{CH}_3)_2\text{CO}$.

Luminescence properties

The PO1 and PO4 ligands were known earlier to form luminescent complexes with terbium acylpirazolonates or beta-diketones,^{16,17} while no data for terbium sensitization ability by PO2 and PO3 are present in the literature. Besides even in the case of PO1 and PO4, it was not clear whether the PO-ligand played a role in the luminescence sensitization, or terbium luminescence was observed due to the anionic ligand. Therefore to test the possibility of terbium luminescence sensitization by these ligands, $\text{TbCl}_3(\text{PO})\cdot\text{H}_2\text{O}$ luminescence was examined.

All the $\text{TbCl}_3(\text{PO})\cdot\text{H}_2\text{O}$ (PO = PO1–PO4) complexes exhibit only terbium ionic luminescence, and the absence of ligand emission bands in the spectrum and high quantum yields (up to 70%, Table 1) indicate a high sensitization efficiency (Fig. 4b). The different Stark splitting of the $^5\text{D}_4 \rightarrow ^7\text{F}_j$ bands in the luminescence spectra of $\text{TbCl}_3(\text{PO})\cdot\text{H}_2\text{O}$ indicates a significant difference in the coordination environment of the terbium ion in these complexes, which is also confirmed by the different lifetimes of the complexes (Table 1).

The excitation spectra of $\text{TbCl}_3(\text{PO})\cdot\text{H}_2\text{O}$ are strongly different from each other (Fig. 4a), which is due to the different energies of the singlet excited states of the PO ligands. The excitation spectrum of $\text{TbCl}_3(\text{PO1})\cdot\text{H}_2\text{O}$ differs

Table 1 Luminescence properties of terbium complexes

Complex	PLQY, % (± 5)	τ_{obs} , ms (± 0.05)
$\text{TbCl}_3(\text{PO1})\cdot\text{H}_2\text{O}$	29	1.25
$\text{TbCl}_3(\text{PO2})\cdot\text{H}_2\text{O}$	54	2.77
$\text{TbCl}_3(\text{PO3})\cdot\text{H}_2\text{O}$	39	2.12
$\text{TbCl}_3(\text{PO4})\cdot\text{H}_2\text{O}$	69	1.89
$\text{Tb}(\text{pobz})_3(\text{PO1})\cdot(\text{CH}_3)_2\text{CO}$	100	1.86
$\text{Tb}(\text{pobz})_3(\text{PO2})\cdot(\text{CH}_3)_2\text{CO}$	87	1.47
$\text{Tb}(\text{pobz})_3(\text{PO3})\cdot(\text{CH}_3)_2\text{CO}$	95	1.73
$\text{Tb}(\text{pobz})_3(\text{PO4})\cdot(\text{CH}_3)_2\text{CO}$	100	1.76

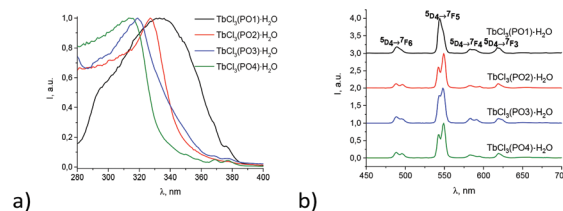


Fig. 4 (a) Excitation ($\lambda_{\text{em}} = 545$ nm) and (b) luminescence ($\lambda_{\text{ex}} = 320$ nm) spectra of $\text{TbCl}_3(\text{PO})\cdot\text{H}_2\text{O}$ complexes.

substantially from the other excitation spectra, which can be attributed to the fundamentally different structure of the PO1 ligand, since it is the only ligand in which the triphenylphosphine oxide fragments are connected through an aliphatic, and not aromatic, bridge (Fig. 1).

The $\text{Tb}(\text{pobz})_3(\text{PO})\cdot(\text{CH}_3)_2\text{CO}$ (PO = PO1–PO4) complexes also exhibit only terbium ionic luminescence (Fig. 5b). The excitation spectra of $\text{Tb}(\text{pobz})_3(\text{PO})\cdot(\text{CH}_3)_2\text{CO}$ are very similar to each other and to the excitation spectrum of the complex $\text{Tb}(\text{pobz})_3(\text{H}_2\text{O})_2$ (Fig. 5a). This suggests that the HOMO and LUMO orbitals in $\text{Tb}(\text{pobz})_3(\text{PO})\cdot(\text{CH}_3)_2\text{CO}$ appear to be localized to the *o*-phenoxybenzoate anion, and it plays an important role in the transfer of energy to the terbium ion.

The quantum yields of $\text{TbCl}_3(\text{PO})\cdot\text{H}_2\text{O}$ allow a qualitative assessment of the sensitization efficiency of ligands, which is rather high for all the ligands. The highest sensitization efficiency was observed for PO4. The quantum yields of all the $\text{Tb}(\text{pobz})_3(\text{PO})\cdot(\text{CH}_3)_2\text{CO}$ complexes reach 87–100% (Table 1), which makes them prospective luminescent materials for various applications. Such high quantum yields of

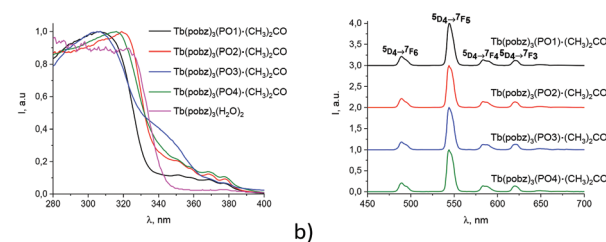


Fig. 5 (a) Excitation ($\lambda_{\text{em}} = 545$ nm) and (b) luminescence ($\lambda_{\text{ex}} = 320$ nm) spectra of $\text{Tb}(\text{pobz})_3(\text{PO})\cdot(\text{CH}_3)_2\text{CO}$ complexes.

Tb(pobz)₃(PO)·(CH₃)₂CO were expected as the PLQY of Tb(pobz)₃(H₂O)₂ reached 96%.¹⁸

Quantum chemical calculations

Quantum chemical modeling was aimed at determining the energies of the frontier orbitals of the neutral ligands, since these values are crucial for OLED fabrication as they are expected to be involved in the electron transport processes. In addition, the localization of frontier orbitals was determined, since the knowledge of the orbital localization would allow the determination of the positions for the substituent introduction for the directed change of the energies of these orbitals.

For the PO2 ligand, the energies of the frontier orbitals have already been calculated by Chunmiao Han *et al.* at the DFT B3LYP/6-31G* level in ref. 12 and were recalculated here by the same dual-stage approach as for PO1, PO3, and PO4 (DFT + TDDFT PBE0/6-31G* level).

According to the DFT results, HOMOs are localized on the linker between the individual phosphine oxides (Fig. 6). This explains the differences in the energy of the HOMO for selected PO1–PO4 compounds, since the nature of the linker is different: aromatic (PO2, PO4), heteroaromatic (PO3), and aliphatic (PO1).

It is well known that the DFT method, suitable for ground state calculations, significantly overestimates the energies of virtual orbitals containing no electrons, to which the LUMO belongs. Therefore in our work we used a dual-stage approach to determine the LUMO energy, based on the calculation of vertical excitations and then the energy gap (E_g) from TDDFT, followed by the calculation of the LUMO energy as $E(\text{LUMO}) = E(\text{HOMO}) + E_g$.

To verify the reasonableness of vertical excitation calculations, the TDDFT absorption spectra were compared with those experimentally observed. It turned out that they correlated very well both in the position of the bands and in the relative magnitude of the oscillator strength (Fig. 7). The high absorption of PO ligands (up to $\epsilon = 5 \times 10^4 \text{ M}^{-1} \text{ cm}^{-1}$, Fig. 7a) also makes Tb(pobz)₃(PO)·(CH₃)₂CO complexes promising for photoluminescence applications.

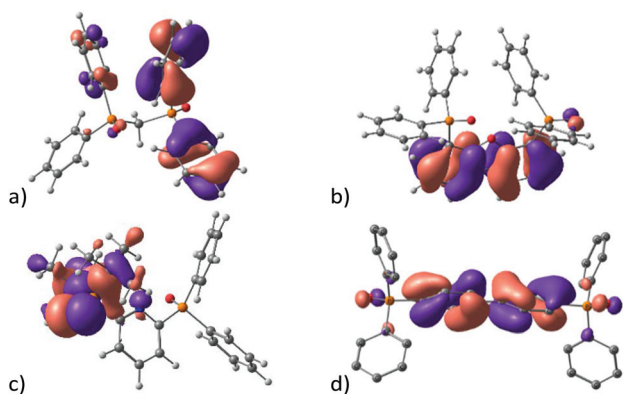


Fig. 6 Localization of the HOMO in arylphosphine oxides: (a) PO1, (b) PO2, (c) PO3, and (d) PO4.

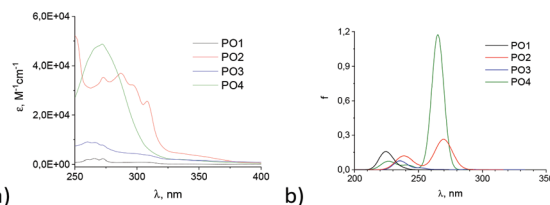


Fig. 7 Absorption spectra of PO: (a) experimental (10^{-5} M , acetonitrile) and (b) calculated.

It was found that only for the PO4 ligand, the lowest energy band in the TDDFT spectrum corresponds to the HOMO \rightarrow LUMO transition. In the remaining cases, all the calculated absorption bands correspond to the superposition of several electronic transitions. The most significant contribution is made by the transitions HOMO–1 \rightarrow LUMO and HOMO \rightarrow LUMO (Table 2). To calculate the energy of the LUMOs, we used the expression $E(\text{LUMO}) = E(\text{HOMO}-N) + E_g$, where $E(\text{HOMO}-N)$ corresponds to either (a) the energy of the orbital with the highest contribution, or (b) the weighted average energy of the orbitals from which the transition to the LUMO was observed.

We found that the energy values obtained from the energy of the main and averaged orbitals (Table 2) practically coincided. At the same time, as expected, the obtained LUMO values differ significantly from the data of the DFT method, particularly the LUMO energy of the PO2 ligand is significantly different from that from ref. 12.

OLED fabrication

The synthesized complexes were tested in OLEDs as emission layers within the composite films Tb(L)₃:nPO (L = Cl[−], pobz[−]; PO = PO1–PO4), where an excess of PO was introduced to ensure electronic mobility, and the ratio of Tb(L)₃:PO = 1:n was varied (Table 3).

The ETL and HTL layers were chosen according to the calculated HOMO and LUMO energy values of the PO. Initially, the TAZ material with a high LUMO energy (2.8 eV) was chosen as the electron transport layer due to the high LUMO level of PO1–PO4. The widely used PVK material was chosen as the hole transport layer, since its HOMO level (5.8 eV) is well suited to facilitate the transport of holes from the PEDOT:PSS hole into the emission layer, as well as PVK is insoluble in ethanol, from which the emission layer will be deposited.

To determine the best host material, all PO1–PO4 hosts were tested in OLEDs with the same heterostructures with TbCl₃:5PO (PO = PO1–PO4) emission layers made under the same conditions (A–D devices, Table 3). In the electroluminescence spectra of all A–D diodes, typical emission bands of terbium luminescence corresponding to the ⁵D₄ \rightarrow ⁷F_J transitions were observed.

The electronic mobility of the PO materials was estimated by comparing the current values at the same voltage from the *I*–*V* curves (Fig. 8b). The mobility increases in the A–C–B–D series and the maximum electronic mobility is demonstrated by the materials PO2 and PO4. The efficiency of the

Table 2 Quantum chemical calculation data

PO =	$E(\text{HOMO}), \text{eV}$	$E(\text{LUMO}) (\text{DFT}), \text{eV}$	E_g, eV	Transition (contribution ^a)	$E(\text{HOMO}-N), \text{eV}$	$E(\text{LUMO})^b, \text{eV}$
PO1	-6.923	-0.917	5.21	HOMO → LUMO (64%) HOMO-1 → LUMO (15%) HOMO-1 → LUMO+1 (15%) HOMO-1 → LUMO+5 (2%) HOMO → LUMO+1 (1%) HOMO → LUMO+2 (3%)	$E(\text{HOMO}) = -6.923$ $E_{\text{avg}1,2} = -6.933$	(a) -1.713 (b) -1.723
PO2	-6.563	-1.295	4.5056	HOMO-1 → LUMO (78%) HOMO → LUMO+2 (14%) HOMO-3 → LUMO (8%)	$E(\text{HOMO}-1) = -6.691$ $E(\text{HOMO}-3) = -6.841$ $E_{\text{avg}} = -6.705$	(a) -2.185 (b) -2.199
PO3	-6.84	-1.262	4.277	HOMO-1 → LUMO (90%) HOMO → LUMO (10%)	$E(\text{HOMO}-1) = -6.876$ $E_{\text{avg}} = -6.841$	(a) -2.599, (b) -2.564
PO4	-6.694	-1.347	4.659	HOMO → LUMO	$E(\text{HOMO}) \equiv E_{\text{avg}} = -6.694$	-2.04

^a Contribution = squared coefficient of Spin Adapted Antisymmetrized Product (SAAP²). ^b LUMO energy estimated as $E(\text{HOMO}-N) + E_g$, where $E(\text{HOMO}-N)$ corresponds to (a) the energy of the main orbital from which the transition occurs, and (b) the weighted averaged energy of the orbitals from which the transition to the LUMO occurs.

PO* → Tb³⁺ electroexcitation transfer was evaluated from the electroluminescence spectra measured at the same current (Fig. 8a). The electroluminescence intensity increases in the A-C-B-D series and corresponds to an increase in the sensitizing ability of the PO ligands which correlates with the values of the quantum yields of TbCl₃(PO)·H₂O complexes (Table 1).

Thus, in our case, the mobility and sensitization efficiencies of the materials of the PO ligands change symbatically in the row PO1-PO3-PO2-PO4 and allow us to choose PO4 as the best material.

To determine the effect of the anionic ligand on the electroluminescence intensity, we replaced terbium chloride with phenoxybenzoate in the composition of the emission layers, and thus E-H devices were obtained (Table 3). It turned out that such a replacement resulted in an increase in the electroluminescence intensity by a factor of 1.5-2, and this behavior was observed for all the investigated hosts (Fig. S41†). Thus, it is shown that in spite of the fact that the exciton is generated on the electron transporting PO material, the excitation is transferred and distributed throughout the whole organic subsystem of Tb(pobz)₃(PO), and the pobz⁻ anionic ligand participates in the energy transfer process toward Tb³⁺.

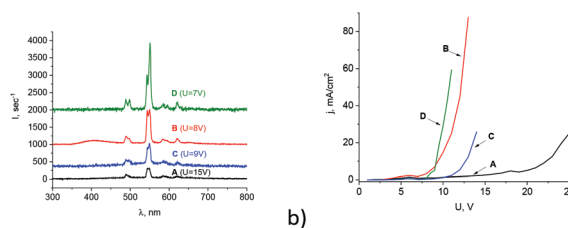


Fig. 8 (a) The electroluminescence spectra and (b) the I - V curves of the devices A-D.

Thus, the best results were observed using Tb(pobz)₃(PO4) as an emitter. The next task was to optimize the structure of this OLED. Variation of the Tb:PO4 ratio in the composition of the emission layer demonstrated that even with a ratio of 1 to 1 (device I, Table 3) the electron mobility of PO4 is sufficient for efficient working of the device, as evidenced by high enough currents (Fig. 9b). The intensity of electroluminescence increases (Fig. 9a), and the maximum luminance reaches 25 Cd m⁻² at 12 V.

The introduction of the LiF electron-injecting layer and the replacement of the electron transport layer TAZ by TPBi, which

Table 3 Device list

Device designation	Heterostructure	$U_{\text{on}}^a, \text{V}$
A	ITO/PEDOT:PSS/PVK/TbCl ₃ :5PO1/TAZ/Al	14
B	ITO/PEDOT:PSS/PVK/TbCl ₃ :5PO2/TAZ/Al	6.5
C	ITO/PEDOT:PSS/PVK/TbCl ₃ :5PO3/TAZ/Al	8
D	ITO/PEDOT:PSS/PVK/TbCl ₃ :5PO4/TAZ/Al	6
E	ITO/PEDOT:PSS/PVK/Tb(pobz) ₃ :5PO1/TAZ/Al	10
F	ITO/PEDOT:PSS/PVK/Tb(pobz) ₃ :5PO2/TAZ/Al	6
G	ITO/PEDOT:PSS/PVK/Tb(pobz) ₃ :5PO3/TAZ/Al	8
H	ITO/PEDOT:PSS/PVK/Tb(pobz) ₃ :5PO4/TAZ/Al	6
I	ITO/PEDOT:PSS/PVK/Tb(pobz) ₃ :1PO4/TAZ/Al	6
J	ITO/PEDOT:PSS/PVK/Tb(pobz) ₃ :1PO4/TPBi/LiF/Al	5

^a As the U_{on} value, the voltage, where EL detectable with the naked eye appeared, was considered.

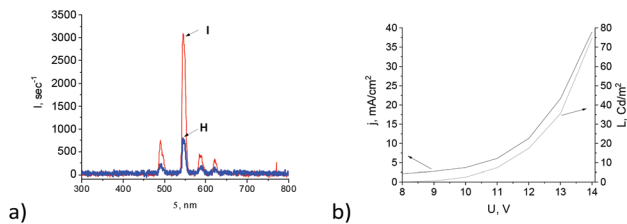


Fig. 9 (a) Electroluminescence spectra of devices H and I at 7 V and (b) I - V and L - V curves of device J.

has higher electron mobility²¹ (device J, Table 3) lead to an increase in currents and in the luminance of the diode, which reaches 75 Cd m⁻² at 14 V (Fig. 9b). Though this value is much below the state-of-the-art values for the vacuum-deposited OLEDs, we believe that it is important to publish it to be able to trace the progress in such a young and prospective area of research as solution-processed OLED development.

Experimental section

Materials and methods

All solvents and chemicals were purchased from commercial sources.

¹H NMR spectra were recorded at 25 °C using an Agilent 400 MR spectrometer with an operating frequency of 400.130 MHz, 100.613 MHz and 376.498 MHz, respectively. Chemical shifts were reported in ppm relative to Me₄Si (¹H). Elemental analysis was performed on the microanalytical device Heraeus Vario Elementar. Thermal analyses were carried out on a thermoanalyzer STA 409 PC Luxx (NETZSCH, Germany) in the temperature range of 20–1000 °C in air, at a heating rate of 10° min⁻¹. The composition of the evolved gases was simultaneously monitored during the TA experiment using a coupled QMS 403C Aeolos quadrupole mass spectrometer (NETZSCH, Germany). The mass spectra were recorded for the species with the following m/z values: 18 (corresponding to H₂O), 44 (corresponding to CO₂), and 58 (corresponding to (CH₃)₂CO).

Powder X-ray diffraction (PXRD) was performed by using Bruker D8 Advance [$\lambda(\text{Cu-K}\alpha) = 1.5418 \text{ \AA}$; Ni filter] and Bruker D8 Advance Vario diffractometers [$\lambda(\text{Cu-K}\alpha_1) = 1.54060 \text{ \AA}$; Ge(111)-monochromator] with a step size of 0.020°. The patterns were indexed by using the SVD-Index²² as implemented in the TOPAS 4.2 software.²³ Then, the powder patterns were refined by using the Pawley method.

Absorption spectra were recorded in the region of 250–800 nm with a PerkinElmer Lambda 650 spectrometer. Emission and excitation spectra were recorded with a Fluorolog 3 spectrofluorometer over excitation with a xenon lamp. Luminescence lifetime measurements were carried out and detected on the same system. Lifetimes are averages of at least three independent measurements. All luminescence decays proved to be perfect single-exponential functions.

Photoluminescence quantum yields were determined with a Fluorolog FL3–22 spectrofluorimeter at room temperature under excitation into ligand states according to an absolute method using an integration sphere. The modified de Mello *et al.*²⁴ method requires the measurement of (i) L_a , the integrated intensity of light exiting the sphere when the empty cuvette is illuminated at the excitation wavelength (Rayleigh scattering band); (ii) L_c , the same integrated intensity at the excitation wavelength when the sample is introduced into the sphere; (iii) E_a the integrated intensity of the entire emission spectrum of the empty cuvette; and (iv) E_c the integrated intensity of the entire emission spectrum of the cuvette with the sample. The absolute quantum yield is then given by:

$$\text{PLQY} = \frac{E_c - E_a}{L_a - L_c} \times 100\%.$$

OLED manufacturing took place in a clean room class 10 000 (Lebedev Physical Institute, Moscow, Russia) in a glove-box under an argon atmosphere. The substrates were cleaned by ultrasonication in the following media: NaOH aqueous solution, distilled water, acetone and 2-propanol for 16 min each.

A 40 nm-thick poly(3,4-ethylenedioxythiophene):poly(styrenesulfonate) (PEDOT:PSS) hole-injective layer was first deposited. An aqueous solution of PEDOT:PSS (5 ml) was poured onto the preheated (70 °C) patterned ITO glass substrate, after which the substrate was rotated for 60 seconds at 2000 rpm. Finally, the deposited film was annealed in air at 80 °C for 60 min. As a hole-transport layer PVK solution was spin-coated from toluene ($c = 5 \text{ g L}^{-1}$).

The emission layer was spin-coated from the solution ($c = 5 \text{ g L}^{-1}$) on the heterostructure or on the glass substrate. The ~30 nm-thick electron-transport/hole-blocking layer (TAZ or TPBi) was thermally evaporated (Univex-300, LeyboldHeraeus) followed by a ~1 nm-thick LiF layer and a >100 nm-thick aluminum layer as the cathode under a pressure below 10⁻⁶ mm Hg. The thickness of the layers was controlled by using a quartz indicator. The contacts were attached to the electrodes, and the device was sealed with epoxy resin (Norland Optical Adhesive).

Electroluminescence spectra were recorded on a PicoQuant time-correlated single photon counting system used as a conventional spectrofluorimeter. The spectral resolution was 4 nm. All the measurements were carried out in the same configuration, which allows quantitative comparison of the spectra by dividing by the integration time.

Quantum chemical calculations. The geometry of the ground state of the PO molecules was optimized using the DFT method with the functional PBE0 and 6-31G* basis set in the NWChem 6.4 package.²⁵ To choose the structural isomer, the geometry of each possible isomer was optimized and the lowest-energy isomer was chosen. The optimized molecular geometries (Table S4†) were checked for the absence of imaginary frequencies in the vibrational spectra (Table S5†).

TDDFT calculations at the same PBE0/6-31G* level as implemented in the Firefly 8.2 package²⁶ were carried out for

the optimized geometry of PO molecules. 20 singlet single-excited states were considered.

The energies of the frontier orbitals were calculated using the DFT and TDDFT results. The energy of the HOMO was obtained as the eigenvalue of DFT calculation for the ground state (Table S6[†]). The energy of the LUMO was computed as described in the Results and discussion section.

Synthesis of PO ligands

Phosphine oxides were obtained by the oxidation of the corresponding phosphines.

Bis(diphenylphosphino)methane (for PO1) was purchased from abcr GmbH.

1,8-Bis(diphenylphosphino)dibenzofuran (for PO2) was prepared as in ref. 27.

MS(FD): 537.1 (M^+), 1072,2 ($M^+ + M$).

The ¹H-NMR spectrum (Bruker, 400 MHz in acetone-d₆) was consistent with ref. 27.

2-Diphenylphosphino-6-di(*tert*-butyl)phosphinopyridine (for PO3).

2,6-Dibromopyridine (6.6 g, 28 mmol) was dissolved in dry THF and stirred for 30 min at -78 °C under an argon blanket. The first portion of *n*-butyllithium (5.5 mL, 28 mmol) was introduced to the solution *via* a syringe. The reaction mixture was stirred at -78 °C for one hour and further stirred for 30 minutes at room temperature. After cooling again to -78 °C, di-*tert*-butylchlorophosphine (5.4 mL, 28 mmol) was added dropwise *via* a syringe, stirring was maintained for 1 h at this temperature, and warmed slowly to 0 °C. The second portion of *n*-butyllithium (5.5 mL of 28 mmol) was introduced after cooling the reaction mixture again at -78 °C. After stirring the reaction mixture for one hour, chlorodiphenylphosphine (5.1 mL, 28 mmol) was added at once. The reaction mixture was warmed up to room temperature within 3 h. The residue obtained after evaporating the solvent was washed with methanol (2 × 40 mL) to remove inorganics.

Bis(diphenylphosphino)-4,4'-biphenyl (for PO4).

4,4'-Dibromobiphenyl (9.36 g, 30 mmol) in THF was stirred at -78 °C for 30 min, while stirring *n*-butyllithium (25 mL, 62.5 mmol) was added dropwise. The reaction mixture was allowed to warm up to 0 °C, then chlorodiphenylphosphine (11.5 mL, 62.5 mmol) was added after cooling again at -78 °C. The reaction mixture was warmed up to room temperature and further stirred for 2 h. The residue obtained after evaporating the solvent was stirred with methanol (2 × 40 mL) to remove inorganics. The precipitate thus obtained was filtered off and dried.

General procedure for the oxidation of phosphines: phosphine oxides were synthesized by the oxidation of the corresponding phosphines. Three equivalents of H₂O₂ (30%) per dioxide were added slowly to the vigorously stirred THF solution of the respective phosphine. Stirring was maintained at room temperature for 2 h. After the evaporation of THF, the residue was treated with acetone/ethyl acetate to obtain the respective phosphine oxide product as a precipitate. The precipitate thus obtained was filtered off and dried in a vacuum.

PO1: Yield = 90%; Bruker ¹H NMR and el. anal. data as in the literature,²⁸ MS(MALDI): $m/z = 416$ ($[M + H]^+$);

PO2: Yield = 90%; Bruker ¹H NMR data as in the literature.¹²

MS(MALDI): 569 ($[M + H]^+$);

Elemental analysis: calcd. C 76.05, H 4.61, found C 76.16, H 4.72.

PO3: Yield = 98%; Bruker ¹H NMR (250 MHz, DMSO-d₆) ppm: 8.19–7.47 (m, 13H, Phen-H and, py-H), 0.96 (s, 18H, 2 *t*-Bu);

MS(MALDI): $m/z = 440$ ($[M + H]^+$);

PO4: Yield = 92%; Bruker ¹H NMR (250 MHz, CDCl₃, TMS) ppm: 7.80–7.43 (m, 28H, Phen-H);

MS(MALDI): $m/z = 555$ ($[M + H]^+$);

Elemental analysis: calcd. C 77.97, H 5.09 found C 77.93, H 5.29.

Synthesis of lanthanide complexes

Synthesis of Ln(pobz)₃(H₂O)₂ (Ln = La, Tb). Ln(pobz)₃(H₂O)₂ (Ln = La, Tb) were synthesized by reaction 1 between stoichiometric amounts of TbCl₃·6H₂O or La(NO₃)₃·6H₂O and Kpobz (*in situ* from Hpobz and KOH) in water. The products were dried in air at room temperature.

Synthesis of LnCl₃(PO)·H₂O (Ln = Gd, Tb; PO = PO1–PO4). LnCl₃(PO)·H₂O (Ln = Gd, Tb; PO = PO1–PO4) were synthesized by the reaction between the corresponding PO and the excess of LnCl₃·6H₂O in ethanol. The products were rotor evaporated to dryness, washed with water from the excess of LnCl₃·6H₂O and dried in air at room temperature.

TbCl₃(PO1)·H₂O: MS(MALDI): $m/z = 645$ ($[TbCl_2(PO1)]^+$).

TbCl₃(PO2)·H₂O: MS(MALDI): $m/z = 797$ ($[TbCl_2(PO2)]^+$).

TbCl₃(PO3)·H₂O: MS(MALDI): $m/z = 668$ ($[TbCl_2(PO3)]^+$).

TbCl₃(PO4)·H₂O: MS(MALDI): $m/z = 783$ ($[TbCl_2(PO4)]^+$).

Synthesis of Ln(pobz)₃(PO)·(CH₃)₂CO (Ln = La, Tb; PO = PO1–PO4). Ln(pobz)₃(PO)·(CH₃)₂CO (Ln = La, Tb) were synthesized by the reaction between stoichiometric amounts of LnCl₃(PO)·H₂O and Kpobz (*in situ* from Hpobz and KOH) in a water–acetone mixture. The precipitated product was dried in air at room temperature.

Tb(pobz)₃(PO1)·(CH₃)₂CO: MS(MALDI): $m/z = 1001$ ($[Tb(pobz)_2(PO1)]^+$).

Tb(pobz)₃(PO2)·(CH₃)₂CO: MS(MALDI): $m/z = 1153$ ($[Tb(pobz)_2(PO2)]^+$).

Tb(pobz)₃(PO4)·(CH₃)₂CO: MS(MALDI): $m/z = 925$ ($[Tb(pobz)(PO4)-H]^+$).

Conclusions

To conclude, in the present work we aimed at the development of a new approach toward host selection for lanthanide-based emitters in OLEDs, earlier proposed by some of us,¹¹ based on the example of terbium-based emitters. As host materials, arylphosphine oxides PO = PO1–PO4 were proposed, which were supposed to both sensitize terbium luminescence and provide electron mobility. To assess their sensitization properties,

TbCl₃(PO)·H₂O complexes were obtained and thoroughly investigated. It was found that their quantum yields reach 70%, indicating their high sensitization ability. The high current in the *I*-*V* curve of the OLED based on these materials together with the pure terbium electroluminescence (EL) spectrum indicated their sufficient electronic properties and, thus, the effectiveness of the proposed approach. To select additional layers in OLEDs, the frontier orbitals of PO ligands were calculated based on a complex approach, which allows careful assessment of not only the ground state orbitals, including the HOMO, but also the virtual LUMO orbital.

Conflicts of interest

There are no conflicts to declare.

Acknowledgements

This work was supported by the Russian Foundation for Basic Research (grants #16-53-76018, #17-32-80050). UV thanks President's grant MK-2810.2017.3 for the financial support. MP thanks National Science Centre, Poland, grant no.: OPUS9 2015/17/B/ST5/01038, in part by the Institute of Physical Chemistry of the Polish Academy of Sciences. The research is carried out using the equipment of the shared research facilities of HPC computing resources at Lomonosov Moscow State University.

Notes and references

- J. Jayabharathi, K. Jayamoorthy and V. Thanikachalam, *J. Organomet. Chem.*, 2014, **761**, 74–83.
- N. Thejo Kalyani and S. J. Dhoble, *Renewable Sustainable Energy Rev.*, 2015, **44**, 319–347.
- L. Duan, L. Hou, T.-W. Lee, J. Qiao, D. Zhang, G. Dong, L. Wang and Y. Qiu, *J. Mater. Chem.*, 2010, **20**, 6392.
- T. W. Lee, T. Noh, H. W. Shin, O. Kwon, J. J. Park, B. K. Choi, M. S. Kim, D. W. Shin and Y. R. Kim, *Adv. Funct. Mater.*, 2009, **19**, 1625–1630.
- L. Deng, W. Li and J. Li, *Displays*, 2013, **34**, 413–417.
- J. C. G. Bünzli and S. V. Eliseeva, in *Comprehensive Inorganic Chemistry II: From Elements to Applications*, 2nd edn, 2013, vol. 8, pp. 339–398.
- H. Xu, Q. Sun, Z. An, Y. Wei and X. Liu, *Coord. Chem. Rev.*, 2015, **293**, 228–249.
- Z. Chen, F. Ding, F. Hao, Z. Bian, B. Ding, Y. Zhu, F. Chen and C. Huang, *Org. Electron. Phys. Mater. Appl.*, 2009, **10**, 939–947.
- O. V. Kotova, V. V. Utochnikova, S. V. Samoylenkov, A. D. Rusin, L. S. Lepnev and N. P. Kuzmina, *J. Mater. Chem.*, 2012, **22**, 4897.
- M. Bredol, U. Kynast and C. Ronda, *Adv. Mater.*, 1991, **3**, 361–367.
- V. V. Utochnikova, N. N. Solodukhin, A. N. Aslandukov, L. Marciniak, I. S. Bushmarinov, A. A. Vashchenko and N. P. Kuzmina, *Org. Electron. Phys. Mater. Appl.*, 2017, **44**, 85–93.
- C. Han, G. Xie, J. Li, Z. Zhang, H. Xu, Z. Deng, Y. Zhao, P. Yan and S. Liu, *Chem. – Eur. J.*, 2011, **17**, 8947–8956.
- P. E. Burrows, A. B. Padmaperuma, L. S. Sapochak, P. Djurovich and M. E. Thompson, *Appl. Phys. Lett.*, 2006, **88**, 1–4.
- A. W. G. Platt, *Coord. Chem. Rev.*, 2017, **340**, 62–78.
- S. Shuvaev, O. Kotova, V. Utochnikova, A. Vaschenko, L. Puntus, V. Baulin, N. Kuzmina and A. Tzivadze, *Inorg. Chem. Commun.*, 2012, **20**, 73–76.
- F. Marchetti, C. Pettinari, A. Pizzabiocca, A. A. Drozdov, S. I. Troyanov, C. O. Zhuravlev, S. N. Semenov, Y. A. Belousov and I. G. Timokhin, *Inorg. Chim. Acta*, 2010, **363**, 4038–4047.
- K. Miyata, Y. Konno, T. Nakanishi, A. Kobayashi, M. Kato, K. Fushimi and Y. Hasegawa, *Angew. Chem., Int. Ed.*, 2013, **52**, 6413–6416.
- A. S. Kalyakina, V. V. Utochnikova, E. Y. Sokolova, A. A. Vashchenko, L. S. Lepnev, R. Van Deun, A. L. Trigub, Y. V. Zubavichus, M. Hoffmann, S. Mühl and N. P. Kuzmina, *Org. Electron. Phys. Mater. Appl.*, 2016, **28**, 319–329.
- V. S. Sastri, J.-C. G. Bünzli, V. R. Rao, G. V. S. Rayudu and J. R. Perumareddi, *Modern aspects of rare earths and their complexes*, Elsevier, Amsterdam, 2003.
- V. V. Utochnikova, A. S. Kalyakina, I. S. Bushmarinov, A. A. Vashchenko, L. Marciniak, A. M. Kaczmarek, R. Van Deun, S. Bräse and N. P. Kuzmina, *J. Mater. Chem. C*, 2016, **4**, 9848–9855.
- S. Valouch, C. Hönes, S. W. Kettlitz, N. Christ, H. Do, M. F. G. Klein, H. Kalt, A. Colsmann and U. Lemmer, *Org. Electron. Phys. Mater. Appl.*, 2012, **13**, 2727–2732.
- A. A. Coelho, *J. Appl. Crystallogr.*, 2003, **36**, 86–95.
- Bruker, *TOPAS 4.2 User Manual*, 2009.
- J. C. De Mello, H. F. Wittmann and R. H. Friend, *Adv. Mater.*, 1997, **9**, 230–232.
- M. Valiev, E. J. Bylaska, N. Govind, K. Kowalski, T. P. Straatsma, H. J. J. Van Dam, D. Wang, J. Nieplocha, E. Apra, T. L. Windus and W. A. De Jong, *Comput. Phys. Commun.*, 2010, **181**, 1477–1489.
- A. A. Granovsky, Firefly version 8, <http://classic.chem.msu.su/gran/firefly/index.html>.
- M. Kranenburg, Y. E. M. van der Burgt, P. C. J. Kamer, P. W. N. M. van Leeuwen, K. Goubitz and J. Fraanje, *Organometallics*, 1995, **14**, 3081–3089.
- S. Kannan, N. Rajalakshmi, K. V. Chetty, V. Venugopal and M. G. B. Drew, *Polyhedron*, 2004, **23**, 1527–1533.